

The following publication Meng, Q., Chi, Y., Zhang, L., Zhang, P., & Sheng, L. (2019). Towards high-level theoretical studies of large biodiesel molecules: an ONIOM/RRKM/Master-equation approach to the isomerization and dissociation kinetics of methyl decanoate radicals [10.1039/C8CP05593A]. *Physical Chemistry Chemical Physics*, 21(9), 5232-5242 is available at <https://doi.org/10.1039/C8CP05593A>.

Towards high-level theoretical studies of large biodiesel molecules: an ONIOM/RRKM/Master-equation approach to the isomerization and dissociation kinetics of methyl decanoate radicals

Qinghui Meng^{a,b}, Yicheng Chi^a, Lidong Zhang^{b,*}, Peng Zhang^{a,*}, Liusi Sheng^b

a. Departmental of Mechanical Engineering, The Hong Kong Polytechnic University, Hung Hom,

Kowloon, Hong Kong

b. National Synchrotron Radiation Laboratory, University of Science and Technology of China, Hefei,

Anhui, China

Corresponding Author:

Peng Zhang

Department of Mechanical Engineering

The Hong Kong Polytechnic University

Hung Hom, Kowloon, Hong Kong

E-mail: pengzhang.zhang@polyu.edu.hk

Fax: (852)23654703 Tel: (852)27666664

Lidong Zhang

National Synchrotron Radiation Laboratory

University of Science and Technology of China

Hefei, Anhui 230029, P.R. China

E-mail: zld@ustc.edu.cn

Fax: (86) 551 65141078 Tel: (86) 551 63607923

Abstract: The isomerization and dissociation reactions of methyl decanoate (MD) radicals were theoretically investigated by using high-level theoretical calculations based on a two-layer ONIOM method, employing the QCISD(T)/CBS method for the high layer and the M06-2X/6-311++G(d,p) method for the low layer. Temperature- and pressure-dependent rate coefficients for involved reactions were computed by using transition state theory and Rice-Ramsperger-Kassel-Marcus/Master-Equation method. The structure-reactivity relationships were explored for the complicated multiple-well interconnected system of ten isomeric MD radicals. Comparative studies of methyl butanoate (MB) and MD were also performed systematically. Results show that the isomerization reactions are appreciably responsible for the population distribution of MD radicals at low and intermediate temperatures, while the β -scission is dominant at higher temperatures. Although the rate constants of MB specific to methyl esters are close to those of MD in certain temperature ranges, MB is unable to simulate most of dissociation reactions for real biodiesels due to its short aliphatic chain. Significant differences of rate constants for isomerization reactions were observed between the calculated results and the literature data, which were estimated by analogy to alkane systems, but the rate constants of β -scissions show generally good agreement between theory and experiment. The current work extends kinetic data for kinetic modeling of isomerization and dissociation reactions of MD radicals, and it serves as a start for the studies of detailed combustion chemistry of practical biodiesels.

Keywords: Chemical kinetics; Methyl decanoate; Dissociation reaction; Isomerization reaction; ONIOM, RRKM, Master equation

1. Introduction

Biodiesel is regarded as one of the most promising fuel alternatives for its renewable and various feedstocks, environmental benefits, and attractive physicochemical properties¹⁻³. It is primarily composed of long-carbon-chain (12-20 carbon atoms) saturated and unsaturated monoesters derived from chemically reacting lipids with an alcohol through transesterification reactions⁴. Compared with biodiesels obtained from animal oils, those from vegetable oils mainly consist of saturated fatty acid methyl or ethyl esters. Biodiesels can be used in pure form or in blends with petroleum diesel at any concentration in most injection pump diesel engines^{1, 5}. Although knowledge about biodiesel combustion characteristics is essential for its applications, only a few combustion chemistry modeling works (specifically on developing detailed reaction mechanisms and their applications to simulating typical combustion parameters) have been done to investigate the combustion of practical biodiesels⁶⁻⁹.

Methyl decanoate [MD, $\text{CH}_3(\text{CH}_2)_8\text{COOCH}_3$], the largest component (65% by mass) in cuphea biodiesel¹⁰, has been proposed as a typical biodiesel surrogate. Its desirable fuel properties (e.g. low vapor pressure and melting point) make it experimentally accessible using traditional techniques. Herbinet et al.¹¹ developed a detailed reaction mechanism (aka detailed kinetic model) of MD based on the reaction mechanisms of n-heptane¹², iso-octane¹³, and methyl butanoate [MB, $\text{CH}_3(\text{CH}_2)_2\text{COOCH}_3$]¹⁴, and by combining specific oxidation properties of methyl esters. Subsequently, Herbinet et al.¹⁵ updated the MD mechanism by adding the sub-mechanisms of the methyl 5-decanoate and methyl 9-decanoate and used it to

explore the combustion of biodiesels in a jet-stirred reactor. Glaude et al.¹⁶ developed a detailed reaction mechanism for esters up to MD based on the EXGAS code for automatically generating reaction mechanisms. It should be noted that the rate constants of recombination and dissociation reactions in these mechanisms were either calculated by analogy to alkanes or derived from the quantitative structure-reactivity relationships¹⁶. In addition, the rate constants of H-abstraction reactions used in these mechanisms were evaluated by using the Evans-Polanyi correlation for hydrocarbons¹⁶. It was found that the overestimated rate constants resulted in faster reaction rates by about a factor of two at 1000K¹⁶. As pointed out by Dievart et al.¹⁷, different prescriptions of rate constants for the reactions involving molecules with the ester functional group result in appreciably different MD oxidation pathways and model predictions to global combustion parameters. Thus, it is essential and urgent to obtain more reliable rate constants of MD reaction systems.

Recent advances in theoretical and computational chemistry enable the accurate evaluation of thermal and kinetic parameters of relatively small molecules. It is known that the extrapolation to the coupled cluster single and double excitation and perturbative triples CCSD(T)/complete basis set(CBS) predicts the energy barriers with uncertainties less than 1.1 kcal/mol¹⁸, and that the extrapolation of quadratic configuration interaction with singles, doubles and perturbative inclusion of triples QCISD(T)/CBS with a sequence of the correlation-consistent, polarized-valence, triple- ζ (cc-pVTZ), and quadruple- ζ (cc-pVQZ) basis sets can evaluate energy barriers with uncertainties around 1.0 kcal/mol¹⁹. Therefore, high-level theoretical studies aiming for understanding the chemical kinetics of realistic

biodiesels have been focused on small surrogate molecules²⁰⁻²². However, Dievart et al.¹⁷ indicated that small methyl esters such as MB are not ideal surrogates to simulate real biodiesel. More recently, Pyl et al.²³ performed the pyrolysis of MD in a bench-scale reactor equipped with a dedicated on-line analysis section with temperature varied from 873K to 1123K and at a fixed pressure of 1.7 bar. They found that MD was largely consumed by H-abstraction reactions, implying that the unimolecular dissociation and the isomerization reactions of MD radicals may become increasingly important at high temperatures.

Whereas the importance of the isomerization and the dissociation reactions of biodiesel radicals, only few studies have been conducted on their theoretical chemical kinetics. The composite method CBS-QB3 was employed by Glaude et al.¹⁶ for energy predictions of some β -scission reactions of small methyl esters, which have an average deviation of ± 1.0 kcal/mol. For biodiesel surrogate molecules with heavy atoms more than 10, energy calculations with the forementioned high-level methods are formidable task due to their intensive computation load. To meet this challenge, a two-layer ONIOM method was developed by Zhang et al.^{24, 25}, aiming to directly calculate the accurate thermos-chemical and chemical kinetic parameters of the practical biodiesel constituents. The method was systematically validated for the H-abstraction reactions of saturated esters $C_nH_{2n+1}COOC_mH_{2m+1}$ ($n = 1-5, 9, 15$; $m = 1, 2$) and unsaturated esters $C_nH_{2n-1}COOCH_3$ ($n = 2-5, 17$) by hydrogen radicals. The predictions for energy barriers and heat of reactions have comparable accuracy with the QCISD(T)/CBS method with deviations being less than 0.15 kcal/mol.

In the present work, the rate constants of the isomerization and dissociation reactions were theoretically investigated for all MD radicals. Density functional theory (DFT) was employed to locate the stationary points on the potential energy surface. Single point energies of all the species considered herein were refined with the two-layer ONIOM method of Zhang et al.²⁴ Rate constants were then computed with the TST-RRKM theory at temperature from 500K to 2500 K and at the pressures of 0.1, 1, 10 and 100 atm. Moreover, a comparative study of the MD radicals herein with the previous studies on MD radicals¹¹ and MB radicals²⁰ was conducted by analyzing the corresponding thermal and kinetic data.

2. Theoretical Methodology

2.1 Potential energy surfaces

The geometry optimizations, vibrational frequencies, and zero-point energies for all of the stationary points on the potential energy surface (PES) of MD radicals were obtained at the M06-2X/6-311++G(d,p) level of theory. The transition states corresponding to desired reaction coordinates were identified by using the imaginary frequencies analysis and visual inspection. For those ambiguous cases, the intrinsic reaction path analysis was utilized to examine the connections of each saddle point to its local minima. All harmonic frequencies used herein are the original data from the density functional theory calculations without using scaling factors²¹.

The higher-level single point energies were calculated by using a two-layer ONIOM method²⁴, employing the QCISD(T)/CBS for the high layer and the M06-2X-favor DFT method for the low layer. The present ONIOM method predicts the high-level energy of the

entire system by its low-level energy with the correction from the difference between the high-level and low-level energies of the chemically active portion (CAP), given by

$$E^{\text{ONIOM}}[\text{High:Low}] = E^{\text{Low}}(\text{R}) + E^{\text{High}}(\text{CAP}) - E^{\text{Low}}(\text{CAP}) \quad (\text{E1})$$

For the isomerization and dissociation reactions of MD radicals, the CAP consists of the active site and two neighboring CH₂ (or CH₃, COO) groups on one side and two neighboring CH₂ (or CH₃, COO) groups on the other side. The ONIOM [QCISD(T)/CBS:DFT] energy is calculated by

$$\begin{aligned} E^{\text{ONIOM}}[\text{QCISD(T)CBS:DFT}] &= E^{\text{ONIOM}}[\text{QCISD(T)/CBS:DFT}]_{\text{DZ} \rightarrow \text{TZ}} \\ &+ \{E^{\text{ONIOM}}[\text{MP2/CBS:DFT}]_{\text{TZ} \rightarrow \text{QZ}} \\ &- E^{\text{ONIOM}}[\text{MP2/CBS:DFT}]_{\text{DZ} \rightarrow \text{TZ}}\} \end{aligned} \quad (\text{E2})$$

where

$$\begin{aligned} E^{\text{ONIOM}}[\text{QCISD(T)/CBS:DFT}]_{\text{DZ} \rightarrow \text{TZ}} &= E^{\text{ONIOM}}[\text{QCISD(T)/TZ:DFT}] \\ &+ \{E^{\text{ONIOM}}[\text{QCISD(T)/TZ:DFT}] \\ &- E^{\text{ONIOM}}[\text{QCISD(T)/DZ:DFT}]\} \times 0.4629 \end{aligned} \quad (\text{E3})$$

$$\begin{aligned} E^{\text{ONIOM}}[\text{MP2/CBS:DFT}]_{\text{TZ} \rightarrow \text{QZ}} &= E^{\text{ONIOM}}[\text{MP2/QZ:DFT}] \\ &+ \{E^{\text{ONIOM}}[\text{MP2/QZ:DFT}] \\ &- E^{\text{ONIOM}}[\text{MP2/TZ:DFT}]\} \times 0.6938 \end{aligned} \quad (\text{E4})$$

$$\begin{aligned} E^{\text{ONIOM}}[\text{MP2/CBS:DFT}]_{\text{DZ} \rightarrow \text{TZ}} &= E^{\text{ONIOM}}[\text{MP2/TZ:DFT}] \\ &+ \{E^{\text{ONIOM}}[\text{MP2/TZ:DFT}] \end{aligned}$$

$$- E^{\text{ONIOM}}[\text{MP2/DZ:DFT}] \times 0.4629 \quad (\text{E5})$$

The ONIOM [QCISD(T)/CBS:DFT] method has been systematically validated in previous theoretical study of H-abstraction reactions of saturated and unsaturated alkyl esters by hydrogen radicals, and its reliability was confirmed through comparisons with the QCISD(T)/CBS results with deviations being less than 0.15 kcal/mol^{24, 25}. More details of the ONIOM method for biodiesels can be found in the literature^{24, 25}. All the calculations were performed by using the Gaussian 09 program²⁶.

2.2 Temperature- and Pressure-dependent kinetics

For the reactions with well-pronounced transition states, the transition state theory (TST) was used for the calculation of rate constants, where the rigid rotor harmonic oscillator (RRHO) assumption was employed for all the internal degrees of freedom except for those low-frequency torsional modes. For each torsional mode, the hindrance potentials as a function of the torsional angle were explicitly obtained at the M06-2X/6-311++G(d,p) level via relaxed potential energy surface scans with a increment angle of 12°. For the reactions involving the transfer of hydrogen atoms, the tunneling effect on the rate constants was routinely taken into account on base of asymmetric Eckart model²⁷.

As will be shown shortly in Section 3, the PES of the isomerization and dissociation reactions of MD radicals consists of multiple interconnected potential wells and multiple product channels. Pressure dependence was calculated by using the multiple-well Master equation analysis with a single-exponential-down model, $\Delta E_{\text{down}} = 200(T/300)^{0.85} \text{ cm}^{-1}$, to approximate the collisional energy transfer probability. This model has been validated in

relevant studies of MB ²¹ and n-butyl ²⁸. The Lennard-Jones (L-J) parameters for MD was approximated by $\sigma = 7.3 \text{ \AA}$ and $\varepsilon = 604.7 \text{ cm}^{-1}$, which has been utilized in the MD system previously ²⁹. For the bath gas Ar, the L-J parameter $\sigma = 3.47 \text{ \AA}$ and $\varepsilon = 78.89 \text{ cm}^{-1}$ was recommended by Hippler et al. ³⁰. Phenomenological rate coefficients were obtained by solving time-dependent RRKM-based master equations ³¹ implemented in the MESS computer program ³².

3. Results and Discussion

3.1 Potential energy surfaces

3.1.1 Representative PESs of MD radicals

The PES for the isomerization and decomposition reactions of MD radicals were constructed and investigated systematically herein. Ten isomeric MD radicals can either undergo isomerization reactions or decompose to smaller compounds via β -scission reactions. Moreover, the isomerization and β -scission reactions of another isomer $\text{CH}_3(\text{CH}_2)_6\text{CHCH}=\text{C}(\text{OH})\text{OCH}_3$ were also explored. The complete PES consisting of multiple, interconnected species wells and multiple product channels is extremely complicated because of the large number of isomerization reactions between all the potential wells. For clarity and simplicity, the PES for each isomer was presented separately by only showing reaction pathways directly connected to it. The energies of the stationary points on the PESs were determined at the ONIOM [QCISD(T)/CBS:DFT]// M06-2X/6-311++G(d,p) level.

The nomenclature of these ten different radicals is consistent with that used in the

previous study¹⁴. To be specific, the radicals $\text{CH}_3(\text{CH}_2)_7\text{CHCOOCH}_3$, $\text{CH}_3(\text{CH}_2)_6\text{CHCH}_2\text{COOCH}_3$, $\text{CH}_3(\text{CH}_2)_5\text{CH}(\text{CH}_2)_2\text{COOCH}_3$, $\text{CH}_3(\text{CH}_2)_4\text{CH}(\text{CH}_2)_3\text{COOCH}_3$, $\text{CH}_3(\text{CH}_2)_3\text{CH}(\text{CH}_2)_4\text{COOCH}_3$, $\text{CH}_3(\text{CH}_2)_2\text{CH}(\text{CH}_2)_5\text{COOCH}_3$, $\text{CH}_3\text{CH}_2\text{CH}(\text{CH}_2)_6\text{COOCH}_3$, $\text{CH}_3\text{CH}(\text{CH}_2)_7\text{COOCH}_3$, $\text{CH}_2(\text{CH}_2)_8\text{COOCH}_3$ and $\text{CH}_3(\text{CH}_2)_8\text{COOCH}_2$ are denoted by MD2J, MD3J, MD4J, MD5J, MD6J, MD7J, MD8J, MD9J, MD10J and MDMJ, respectively. The isomer $\text{CH}_3(\text{CH}_2)_6\text{CHCH}=\text{C}(\text{OH})\text{OCH}_3$ is denoted by R11.

The PES for MD2J is displayed in Fig. 1, where the β -scission reaction forming n-heptane radicals and methyl acrylate was chosen as the entrance channel. The other β -scission reactions leading to $\text{CH}_3(\text{CH}_2)_7\text{CH}=\text{C}=\text{O}$ and CH_3O has a very high energy barrier compared with the other reactions in the PES and therefore is not shown for clearer presentation. For all the reaction channels in this and the subsequent PESs, the energies are relative to that of MD2J, which was chosen as a reference and defined as zero. As shown in Fig.1, MD2J can isomerize to MD3J, MD4J, ..., MD10J, and MDMJ via 1, 2-, 1, 3-, ..., 1, 8-, and 1, 4- hydrogen migration reactions respectively, with energy barriers ranging from 17.1 kcal/mol to 39.2 kcal/mol. MD2J can isomerize to R11 because of the conjugation effect as result of the overlap of p-orbitals of radical site with the adjacent π -bond of the carbonyl group. However, the energy barrier of the isomerization reaction is as high as 42.1kcal/mol due to the strong steric effect.

The strain energy and the steric effect have critical influence on the energy barrier for the isomerization reactions. When the number of atoms of the ring is larger than 6, the strain energy of the transition state ring remains nearly unchanged and thus the energy barrier is

determined by the steric effect. The steric effect is stronger and the energy barrier is higher for the transition state ring (such as TS2, TS4, TS6, TS8) with an even number of atoms than that (such as TS1, TS3, TS5, TS7) with an odd number of atoms. As shown in Fig.1, the energy barriers of isomerization reactions from MD2J to MD3J, MD4J, MD5J, MD6J, MD7J, MD8J, MD9J, MD10J and MDMJ are 39.2kcal/mol (TS1), 37.7kcal/mol (TS2), 23.9kcal/mol (TS3), 17.1kcal/mol (TS4), 17.6 kcal/mol (TS5), 20.7kcal/mol (TS6), 20.6 kcal/mol (TS7), 28.0kcal/mol (TS8), and 31.0 kcal/mol (TS9), respectively. It is seen that the reaction of MD2J→MD6J (via TS4) through a 5-centered ring transition state is the most energetically favorable one with the lowest energy barrier 17.1kcal/mol. The reaction of MD2J→MD7J through a 6-centered ring transition state (TS5) has an increased energy barrier of 17.6kcal/mol. In comparison with corresponding alkyl radicals, for which the trend of energy barriers increasing with the ring size was reported in the literature³², MD radicals show a non-monotonic trend due to the reduction of symmetry for the existence of ester moieties.

For the reaction without the ester functionality in the transition state ring, the energy barrier decreases and then increases as the size of the transition state ring increases. This is because the ester functional moieties will strengthen the steric effect if they are not included in the transition state ring. This is also observed in other MD radicals, such as the MD3J, whose PES is shown in Fig. 2. The downtrend of the energy barrier is attributed to the lower strain energy with increasing the size of the transition state ring, and the uptrend is caused by stronger steric effect with increasing the size of the transition state ring, as discussed above.

The PES of MD3J is shown in Fig. 2, where two important dissociation reactions are the β -scission reactions forming $\text{CH}_3(\text{CH}_2)_6 + \text{CH}_2=\text{CHCH}_2\text{C}(=\text{O})\text{CH}_3$ (via TS50) and $\text{CH}_3(\text{CH}_2)_6\text{CH}=\text{CH}_2 + \text{C}(=\text{O})\text{OCH}_3$ (via TS51) with the transition state energy of 35.5 kcal/mol and 36.2 kcal/mol, respectively. It is found that the isomerization reaction of MD3J \rightarrow MD8J with the lowest transition state (TS15) energy of 19.4 kcal/mol, which is lower than those of the two β -scission reactions by about 16 kcal/mol. However, the reaction of MD3J \rightarrow MD8J is expected to be kinetically unfavorable unless the temperature is sufficiently low because the TS15 has a tight, 7-membered ring structure. Similar trends have also been confirmed for other MD radicals such as MD4J, ..., MD10.

The PES of MDMJ is shown in Fig. 3. For the reactions involving MDMJ, the transition state ring contains the ester functionality, and the energy barrier decreases as increasing the size of the transition state ring. This is because the strain energy increases with the inclusion of ester functionality in the transition state ring. The isomerization reaction from MDMJ to MD9J (via TS47) has the second lowest transition state energy 24.8 kcal/mol, which can compete with MDMJ \rightarrow MD8J (via TS44) with the lowest transition state energy 20.3 kcal/mol at low temperatures. As temperature increases, the dominant channel for MDMJ is the β -scission reaction producing P16 via a much looser transition state (TS64) than those of the isomerization reactions. All the relative energies of transition states for all isomerization reactions connected ten MD radicals are listed in the Table S2 in *Supplementary Material*.

3.1.2 Discussion on Energies of MD radicals

As mentioned in Introduction, the previous reaction mechanisms of MD were mainly

developed from analogy to alkanes and MB due to the scarce of theoretical kinetic data for large esters ¹¹. In fact, the activation energies of isomerization reactions of MD radicals were estimated by the sum of the activation energy of the corresponding H-abstraction and the strain energy of the transition state ring in the isomerization ^{11, 12}. Although the effect of the ester functionality on the activation energy of the H-abstraction reaction forming MD2J has been estimated, the deviations of activation energy for the H-abstraction reactions forming other MD radicals are larger than 2.0 kcal/mol ¹². The kinetic parameters used in the previous reaction mechanisms are believed to cause significant uncertainties for isomerization reactions of biodiesels, even without showing rate constants in this section.

On the potential energy surfaces, the C-H β -fissions of MD radicals are generally characterized by high energy barriers and therefore will not included in the following discussions. Consequently, the β -scission reaction hereinafter refers to the C-C β -fissions of MD radicals. Energy barriers of the β -scission reactions ranging from 31.6 to 38.7 kcal/mol are comparable with each other but generally higher than those of isomerization reactions. As the ester moieties in MD radicals have a vital influence on the β -scission reactions, the energies barriers and available literature data for energetically favourable reaction channels are summarized in Table 1 for comparison. Available data of MB and n-decane from the previous studies are also listed in Table 1 for comparison.

For MD2J and MB2J, which are located in the α position from the ester moiety, and for MDMJ and MBMJ, which are alkoxy radicals, comparable energy barriers of their dissociation reactions were observed respectively for the specific conjugation effect. Huynh

et al.²⁰ investigated the isomerization and dissociation reactions of MB radicals at the BH&HLYP/cc-pVTZ level. The energy barriers of β -scissions of MB2J and MBMJ are 33.0 and 33.9 kcal/mol, which are higher than those of corresponding MD radicals by 1.3 kcal/mol. Moreover, the dissociation energy barriers of MD2J and MDMJ are in good agreement with available literature data¹⁶ by discrepancies being less than 0.5 kcal/mol. It is recognized that the effect of ester functional group diminishes rapidly with be away from the reaction center. Thus, the dissociation reactions of MD radicals located in the position farther than MD5J to the ester functionality have similar behavior with those of corresponding n-decane radicals³³, with deviations being less than 1.0 kcal/mol. For simplicity, only those energetically favorable reactions with transition states less than 37.0 kcal/mol were implemented in the rate constant calculations in this work.

3.1.3 Discussion on Entropies of MD radicals

To facilitate the discussion on rate constants in the following section, entropies of MD radicals will be briefly discussed here. The pre-exponential factor (aka A-factor) in the rate coefficient expressions of TST is thermodynamically related to the entropy change ($\Delta S^\ddagger = S^\ddagger - S_R$) from the reactants to the transition state. A tight transition state commonly has a smaller entropy than a loose transition state. The ΔS^\ddagger at 298.15 K for isomerization and dissociation reactions for MD radicals are listed in the Table S3, where the corresponding reactions for MB radicals are listed for comparison.

For transition state without the ester functionality in the transition state ring, an example is shown in Fig. S1. The ΔS^\ddagger of the reactions from MD2J to MD3J, MD4J, MD5J, MD6J,

MD7J, MD8J, and MD9J are -2.6cal/mol, -5.1cal/mol, -7.0cal/mol, -11.3cal/mol, -12.9cal/mol, -14.8cal/mol, -17.4cal/mol and -16.3cal/mol, respectively, where the ΔS^\ddagger decreases with increasing the transition state ring size. The ΔS^\ddagger of isomerization reactions from MD2J to MD10J is -4.1cal/mol higher than that of the reaction from MD2J to MD9J. This is caused by the different electronic interaction of MD10J, where the radical is located at the terminal site. Compared with the similar reactions in the MB system, the ΔS^\ddagger for the MD reactions are higher due to the longer aliphatic chain.

For transition state with the ester functionality in the transition state ring, an example is shown in Fig. 2. The ΔS^\ddagger of the reactions from MD2J, MD3J, MD4J, MD5J, MD6J, MD7J, MD8J, and MD9J to MDMJ are -4.1cal/mol, -6.1cal/mol, -10.5cal/mol, -13.8cal/mol, -15.4cal/mol, -18.5cal/mol, -22.4cal/mol and -22.8cal/mol, respectively. The ΔS^\ddagger of the reaction from MDMJ to MD10J is -18.5 cal/mol higher than that of the reaction from MDMJ to MD9J, which is also attributable for the different electronic interaction of MD10J, where the radical is located at the terminal site. The comparison shows that the ΔS^\ddagger for the MD reactions are lower than those for the similar MB reactions, again because of the longer aliphatic chain of the formers.

In addition, the ΔS^\ddagger in the β -scission reactions of other MD radicals are higher in comparison with the MB radicals. The exceptional case is that the ΔS^\ddagger of -2.9cal/mol in the β -scission reaction of MD2J forming P1 is lower by 5.1cal/mol than that of the corresponding β -scission reaction of MB2J due to the strengthened conjugation effect caused by the longer aliphatic chain of MD.

3.2 High-pressure rate constants

3.2.1 Effects of ester functionality

Because kinetic parameters of large methyl esters were mostly obtained by analogy to corresponding alkanes in the previous studies¹⁶, its comparison between the direct calculation by using the ONIOM method and the transition state theory and the evaluation values will be discussed first. As described above, the alkoxy radical, such as MDMJ, and the radical located in the α -site in terms of the ester functionality, such as MD2J, are representative radicals because of the involved ester functional group. Scarcely available kinetic parameter of MD makes the direct comparison impossible. Thus, the reactions involving these representative radicals, such as MD2J and MB2J, MDMJ and MBMJ, were chosen respectively to show the similarity and difference between the isomerization reactions MD2J \rightarrow MDMJ and MB2J \rightarrow MBMJ, as well as that between the β -scission reaction of MD2J \rightarrow P1 and MB2J \rightarrow P. The isomerization reactions MDMJ \rightarrow MD2J and MBMJ \rightarrow MB2J, as well as the β -scission reaction of MDMJ \rightarrow P16 and MBMJ \rightarrow P were also shown for comparison.

Fig. 4 shows high-pressure limit rate coefficients for the representative (a) isomerization and (b) dissociation reactions of MD2J. Relevant kinetic data of some isomerization and β -scission reactions for MB radicals by Huynh et al.²⁰ and for MD radicals by Herbinet et al.¹¹ are also shown for comparison. The temperature range considered in this work was split into two temperature regimes to facilitate the comparison. It is seen that the rate constants of MD2J \rightarrow MDMJ are close to those of MB2J \rightarrow MBMJ only in a narrow temperature range around 2000K. The one-order-of-magnitude difference of rate constants between MD2J \rightarrow

MDMJ and MB2J→MBMJ is observed at temperature less than 800K, due to their energy difference. At low temperatures, the rate constants of MB2J→P are lower than those of MD2J→P1, whereas the rate constants of MD2J→P1 obtained by Glaude et al.¹⁶ agree well with the present results. As shown in Table 1, the energy barrier of MD2J→P1 by this work and by Glaude et al.¹⁶ are 31.6 and 31.2, respectively.

Fig. 5 shows the high-pressure limit rate coefficients for the representative (a) isomerization and (b) dissociation reactions of MDMJ. At temperature below 700K, the rate constants of MDMJ→MD2J (with the energy barrier 26.3 kcal/mol) are close to those of MBMJ→MB2J (with the energy barrier 26.9 kcal/mol) by Huynh et al.²⁰ and are significantly higher than those of MDMJ→MD2J by Herbinet et al.¹¹. For the β -scission reaction, the rate constants of MDMJ→P16 (with the energy barrier 33.2kcal/mol) are close to those of MBMJ→P (with energy barrier 33.9kcal/mol) at low temperatures, but they differ from each other by a factor of 50 at temperature of 2500K. As discussed above, the large difference of the β -scission reactions between the MBMJ and MDMJ is caused by their entropy difference. The entropy change for MDMJ→P16 is -5.8 cal/mol and lower than that for MBMJ by 4.7 cal/mol, which is attributable for the large difference of rate constants at high temperatures. Additionally, the rate constant of MDMJ→P16 by Herbinet et al.¹¹ is higher than the present calculation results by one order of magnitude, probably because they underestimated the energy barriers obtained by analogy to alkanes.

3.2.2 Comparison with alkyls

The ester moiety has significant effects on the reactivity of adjacent groups by strong

conjugation and its influence is reduced dramatically as the aliphatic chain increases. Thus, it is feasible to construct biodiesel kinetic mechanisms based on the rate constants of corresponding alkanes. Fig. 6 (a) is the illustration of difference for the isomerization reactions of (a) MDMJ→MD3J and (b) MD10J→MD7J between the calculated and estimated rate coefficients at high pressure limit^{11 20}. In the present system, MD10J with its radical position at the terminal site of the aliphatic chain is most similar to an alkyl radical. The isomerization reaction of MD10J→MD7J was thereby used to illustrate the kinetic difference as result of using the analogous method. It is seen that the rate constants for MD10J→MD7J obtained by analogy to alkanes are higher than the present results and the difference between them decreases as temperature increases. At low and intermediate temperatures, isomerization reactions play an important role, and the kinetic parameters of isomerization reactions by analogy to alkanes may cause different low-temperature behaviors.

Although MDMJ is a typical radical of methyl ester, the rate constant of the isomerization from MDMJ to MD3J was approximated to be close to that of alkane radicals in MD combustion modeling¹¹. Thus, the isomerization reaction of MDMJ→MD3J was chosen to examine the difference caused by approximation methods. As illustrated in Fig.6 (b), the difference of the rate constants for MDMJ→MD3J between the MD combustion modeling and the present results can be as large as three orders of magnitude at 500K and decreases as temperature increases. This indicates that it is unreliable to produce rate constants by analogy to n-decane for these isomerization reactions. As discussed above in

Section 3.1, the significantly different energy barriers of isomerization reactions between the alkane and methyl ester systems are attributable for the huge difference. Consequently, the approximation method used to estimate the rate constants is questionable, especially for the radicals surrounded by the ester functionality.

The comparison between the present predictions to the rate constants of β -scission reactions of MD4J and MD10J and the available literature data ^{11, 20} are shown in Fig.7. It is seen that, at intermediate and high temperatures, the present predictions of the β -scission reactions of MD4J \rightarrow P5 are close to those of MB4J reported by Huynh et al. ²⁰ and those of MD4J of Herbinet et al. ¹¹. For the β -scission reaction of MD10J \rightarrow P15 at low temperatures, the calculated rate constants are close to those derived from alkanes by using the approximation methods. Their discrepancy becomes increasingly large with increasing temperature.

Based on the discussion above, it is reasonable to predict the rate constant of MDMJ \rightarrow MD2J and its reverse reaction by analogy to the biodiesel surrogate MB²⁰, but the rate constants of other isomerization reactions in the MD system could bring huge uncertainties if they are derived from the alkanes and MB¹¹. Moreover, the rate constants of β -scission reactions are distinguished at low temperatures due to different energy barriers and at high temperatures due to different entropies. This can explain that the rate constants of β -scission reactions in MD system obtained by analogy to alkanes and MB is sometime reasonable since these β -scission reactions have comparable energy barriers.

3.3 Pressure-dependent rate constants

3.3.1 Pressure-dependence of the reactions of MD2J

The pressure-dependent rate constants for three representative reactions of MD2J are illustrated in Fig. 8, where the pressure-dependent rate plots at intermediate and high temperatures have been zoomed in to manifest their difference. It is found that there is no significant pressure dependence in the lower temperature range of 500K-900K, as we anticipated. At higher temperatures, the rate constants can be different from their high-pressure limits by several times. The temperature threshold for considering the pressure dependence decreases with increasing pressure.

It is seen that the pressure-dependent rate plots end at certain temperatures due to the well merging phenomena in the reaction system³³. At sufficiently high temperatures, it is common for some of the radical isomers (i.e. potential wells) to rapidly equilibrate with each other or with bimolecular products. The phenomena of “well merging” occur when the rate of isomerization (or dissociation) reaction from one well to another well becomes comparable to the rate of its internal energy relaxation due to the molecular collision. Consequently, beyond the temperature at which the well merging occurs, the merged wells become chemically indistinguishable and should be considered as a “combined” well, and the total number of wells in the PES is accordingly reduced by one. In the present work, the well-reduction based on the multi-well master equation analysis will not be discussed in detail, and a recently developed method that automates this reduction process has been incorporated into the MESS computer code.

Regarding the pressure dependence of the rate constants at all pressures considered in

this work, the branching ratios of reactions from the MD2J at 0.1 atm, 1 atm, 10 atm and 100 atm are shown in Fig. 9. Although branching ratios of main isomerization reactions decline rapidly with the temperature increases, they are the predominant consumption at low temperatures. In contrast, the branching ratio of the β -scission (MD2J \rightarrow P1) has a rapid growth and reaches approximate equilibrium at sufficiently high temperatures. More than 90% of MD2J is consumed by the β -scission at higher temperatures. At temperature from about 600 to 800K, isomerization and dissociation reactions are comparably important. Therefore, the distribution of MD radicals depends on not only the initial steps but also the isomerization reactions, which may affect the autoignition properties of biodiesels.

3.3.2 Pressure-dependence of the reactions of MD3J

The pressure-dependent rate coefficients for kinetically favourable reactions from MD3J are shown in Fig. 10. The trend of these rate coefficients are overall similar to that of MD2J. For isomerization reactions from MD3J, there is no significant pressure dependence at temperature below 1000K and moderate pressure dependence can be seen in evidence at temperature above 1100K. The well merging temperature for isomerization reactions from MD3J to MD7J increases from 1000K at 0.1 atm to 2000K at 10 atm.

Branching ratios of the reactions for MD3J at 0.1atm, 1 atm, 10 atm and 100 atm are shown in Fig. 11. The rate constants of P3 formation are slightly higher than those of P1 formation at low temperatures due to its higher energy barrier. At high temperatures, the P2 formation becomes more competitive in the consumption of MD3J. As pressure increases, the rate coefficients of the dissociation reactions increase to approach their high pressure limits.

3.3.3 Pressure-dependence of the reactions of MDMJ

Fig.12 shows the temperature- and pressure-dependent rate coefficients of kinetically favorable reactions of MDMJ. The well merging temperature is about 900K at 0.1 atm and increases to 2400K at 100atm. No well merging was observed for MDMJ→MD2J and MDMJ→MD3J at 100 atm below 1400K. As discussed above, the pressure dependence for the rate coefficients at these pressures is moderate, since the well is difficult to stabilize at higher temperatures. The obvious pressure fall-off at 1atm starts at temperature about 900K by a factor of about 3. The significant fall-off indicates that most of the entrance channel flux returns to the MDMJ radicals at high temperatures.

The temperature-dependent branching ratios for the reactions of MDMJ at 0.1 atm, 1atm, 10 atm and 100 atm are shown in Fig. 13. For temperatures from 500K to 1400K, the dominant reaction channels are the isomerization reactions from MDMJ radicals with overall branching ratio being about 60%. The branching ratio of the isomerization from MDMJ to MD2J increases with temperature, reaches the maximum at 1000K, and then declines with further increasing temperature. Eventually, this isomerization reaction vanishes at 1400K due to the well merging. As can be seen in the PES, there is no direct connection between P1 and MDMJ. As temperature increases, branching ratios for the P1 formation increase slowly at first and then has a rapid growth at temperature above 1300K. The branching ratios of the β -scission reaction from MDMJ to P16 remain low at low temperature and then grow up slowly at temperature above 1400K. It can be concluded that 90% of MDMJ radicals were isomerized and decomposed to the P1 and P16 at high temperature. Furthermore, it is also

shown that the branching ratios for the isomerization reaction to MD3J declines with increasing temperature, while those for the reaction to MD2J become more competitive as temperature increases.

Pressure-dependent rate coefficients of reactions for all the MD radicals are given in the *Supplemental Material*. The calculated rate constants of key reactions fitted in the Arrhenius form are given in Table 2.

4. Conclusions

In the present theoretical study, the rate constants of the isomerization and dissociation reactions for methyl decanoate radicals were calculated by using the transition state theory. High-level two-layer ONIOM method was employed to predict single point energies of all the reactions considered. Phenomenological rate constants of the isomerization and dissociation reactions of methyl decanoate radicals were obtained by the RRKM/ME theory. In addition to provide accurate rate constants for the kinetic modeling of practical biodiesel combustion, the explored reactivity-structure relationships for the isomerization and dissociation reactions of MD radicals can be applied to realistic biodiesel combustion chemistry. At intermediate temperatures, intense competitions between isomerization and dissociation reactions, determining the distribution of MD radicals, are of great significance to the autoignition. At temperature higher than 1100K, the chemical kinetics of MD radicals is well described by the dissociation via β -scissions. Moreover, the significant pressure dependence of rate constants was observed for isomerization and dissociation reactions of MD radicals.

Compared with the available literature data of MB, n-decane, and MD, great discrepancies between MB and MD have been found for the reactions specific to methyl esters. The present results suggest that kinetic parameters used in MD modeling by analogy to corresponding alkanes have significant errors for isomerization reactions, whereas they are approximately suitable for simulating the β -scission reactions of MD because of the comparable energy barriers. Theoretical studies focusing on the isomerization and dissociation reactions of MD radicals provide deep insight of its combustion chemistry, which is also beneficial to improve the chemical kinetic modeling of biodiesel oxidation.

Acknowledgements


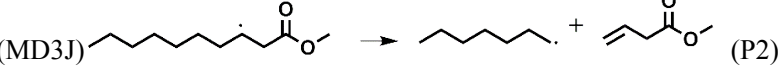
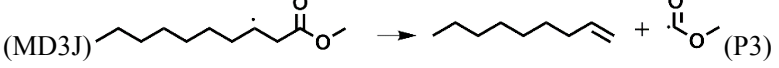





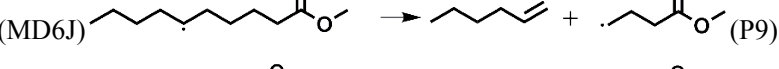
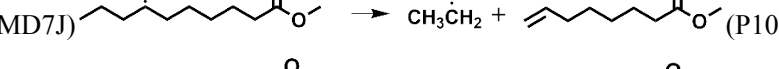

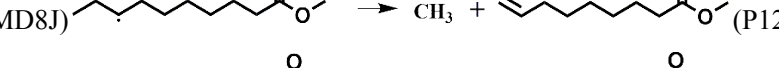



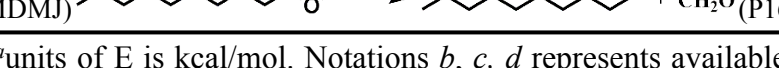
The work at the Hong Kong Polytechnic University was supported by NSFC (No. 91641105), RGC/ECS (PolyU 5380/13E), and SRFDP & RGC ERG Joint Research Scheme (M-PolyU509/13). The work at University of Science and Technology of China was supported by, Natural Science Foundation of China (51676176, U1532137, 11575178 and 21373193), National Key Scientific Instruments and Equipment Development Program of China (2012YQ22011305), and Fundamental Research Funds for the Central Universities (WK2320000038)

References

1. A. K. Agarwal, *Prog. Energy Combust. Sci.*, 2007, 33, 233-271.
2. K. Kohse-Hoinghaus, P. Osswald, T. A. Cool, T. Kasper, N. Hansen, F. Qi, C. K. Westbrook and P. R. Westmoreland, *Angew Chem Int Ed Engl*, 2010, 49, 3572-3597.
3. J. Y. W. Lai, K. C. Lin and A. Violi, *Prog. Energy Combust. Sci.*, 2011, 37, 1-14.
4. L. Meher, D. V. Sagar and S. Naik, *Renew. Sust. Energ. Rev.*, 2006, 10, 248-268.
5. G. Knothe, *Prog. Energy Combust. Sci.*, 2010, 36, 364-373.
6. C. V. Naik, C. K. Westbrook, O. Herbinet, W. J. Pitz and M. Mehl, *Proc. Combust. Inst*, 2011, 33,

- 383-389.
7. C. K. Westbrook, C. V. Naik, O. Herbinet, W. J. Pitz, M. Mehl, S. M. Sarathy and H. J. Curran, *Combust Flame*, 2011, 158, 742-755.
 8. S. Bax, M. H. Hakka, P.-A. Glaude, O. Herbinet and F. Battin-Leclerc, *Combust Flame*, 2010, 157, 1220-1229.
 9. Q. Meng, X. Zhao, L. Zhang, P. Zhang and L. Sheng, *Combust Flame*, 2018, 196, 45-53.
 10. G. Knothe, S. C. Cermak and R. L. Evangelista, *Energ. Fuel*, 2009, 23, 1743-1747.
 11. O. Herbinet, W. J. Pitz and C. K. Westbrook, *Combust Flame*, 2008, 154, 507-528.
 12. H. J. Curran, P. Gaffuri, W. J. Pitz and C. K. Westbrook, *Combust. Flame*, 1998, 114, 149-177.
 13. H. J. Curran, P. Gaffuri, W. J. Pitz and C. K. Westbrook, *Combust Flame*, 2002, 129, 253-280.
 14. E. M. Fisher, W. J. Pitz, H. J. Curran and C. K. Westbrook, *Proc. Combust. Inst.*, 2000, 28, 1579-1586.
 15. O. Herbinet, W. J. Pitz and C. K. Westbrook, *Combust Flame*, 2010, 157, 893-908.
 16. P. A. Glaude, O. Herbinet, S. Bax, J. Biet, V. Warth and F. Battin-Leclerc, *Combust Flame*, 2010, 157, 2035-2050.
 17. P. Diévert, S. H. Won, J. Gong, S. Dooley and Y. Ju, *Proc. Combust. Inst.*, 2013, 34, 821-829.
 18. E. Papajak and D. G. Truhlar, *J. Phys. Chem.*, 2012, 137, 064110.
 19. J. Zádor, C. A. Taatjes and R. X. Fernandes, *Prog. Energy Combust. Sci.*, 2011, 37, 371-421.
 20. L. K. Huynh and A. Violi, *J. Org. Chem.*, 2008, 73, 94-101.
 21. L. Zhang, Q. Chen and P. Zhang, *Proc. Combust. Inst.*, 2015, 35, 481-489.
 22. X. Zhou, Y. Zhai, L. Ye and L. Zhang, *Sustainable Energy & Fuels*, 2017, DOI: 10.1039/C7SE00426E.
 23. S. P. Pyl, C. M. Schietekat, K. M. Van Geem, M.-F. Reyniers, J. Vercammen, J. Beens and G. B. Marin, *Journal of Chromatography A*, 2011, 1218, 3217-3223.
 24. L. Zhang and P. Zhang, *Phys Chem Chem Phys*, 2015, 17, 200-208.
 25. L. Zhang, Q. Meng, Y. Chi and P. Zhang, *J. Phys. Chem. A*, 2018.
 26. M. Frisch, G. Trucks, H. B. Schlegel, G. Scuseria, M. Robb, J. Cheeseman, G. Scalmani, V. Barone, B. Mennucci and G. Petersson, *Inc., Wallingford, CT*, 2009, 200.
 27. C. Eckart, *Physical Review*, 1930, 35, 1303.
 28. P. Zhang, S. J. Klippenstein and C. K. Law, *J Phys Chem A*, 2013, 117, 1890-1906.
 29. P. Diévert, S. H. Won, S. Dooley, F. L. Dryer and Y. Ju, *Combust Flame*, 2012, 159, 1793-1805.
 30. H. Hippler, J. Troe and H. Wendelken, *J. Chem. Phys.*, 1983, 78, 6709-6717.
 31. S. J. Klippenstein and J. A. Miller, *J. Phys. Chem. A*, 2002, 106, 9267-9277.
 32. B. Sirjean, E. Dames, H. Wang, W. Tsang, *J. Phys. Chem. A*, 2012, 116, 319-332.
 33. Y. Georgievskii, J. A. Miller, M. P. Burke and S. J. Klippenstein, *J. Phys. Chem. A*, 2013, 117, 12146-12154.
 34. L. Zhao, T. Yang, R. I. Kaiser, T. P. Troy, M. Ahmed, D. Belisario-Lara, J. M. Ribeiro and A. M. Mebel, *J. Phys. Chem. A*, 2017, 121, 1261-1280.

Table 1. Energy barriers of β -scission reactions for MD radicals ^a.

Reactions	E	Ref.	Deviation
(MD2J) 	31.6	33.0 ^b ,31.2 ^d	1.4 ^b ,0.4 ^d
(MD3J) 	30.0	27.8 ^d	2.2 ^d
(MD3J) 	30.6	33.5 ^b	2.9 ^b
(MD4J) 	30.0	28.7 ^d	1.3 ^d
(MD4J) 	25.0	26.5 ^b	1.5 ^b
(MD5J) 	29.7	29.6 ^c	0.1 ^c
(MD5J) 	30.6	30.1 ^c	0.5 ^c
(MD6J) 	30.0	29.6 ^c	0.4 ^c
(MD6J) 	29.9	29.6 ^c	0.3 ^c
(MD7J) 	29.7	28.9 ^c	0.8 ^c
(MD7J) 	30.2	30.1 ^c	0.1 ^c
(MD8J) 	30.6	29.6 ^c	1.0 ^c
(MD8J) 	29.9	29.9 ^c	0.0 ^c
(MD9J) 	29.8	29.6 ^c	0.2 ^c
(MD10J) 	30.0	29.4 ^c	0.6 ^c
(MDMJ) 	33.2	33.9 ^b ,31.9 ^d	0.7 ^b ,1.3 ^d

^aunits of E is kcal/mol. Notations *b*, *c*, *d* represents available data of MB, n-decane and MD radicals from previous studies of Huynh et al. ²⁰, Zhao et al. ³⁴, and Glaude et al. ¹⁶, respectively.

Table 2. Rate constants of key reactions for MD radicals at high pressure limit ^a.

Reactions	<i>A</i>	<i>n</i>	<i>E_a</i>	Reactions	<i>A</i>	<i>n</i>	<i>E_a</i>
MD2J→6J	3.8E3	1.5	13.9	MDMJ→2J	3.7E9	0.8	25.1
MD2J→7J	7.8	2.6	13.2	MDMJ→3J	3.1E5	1.7	20.7
MD3J→7J	1.1E2	1.8	12.3	MD2J→P1	3.1E11	0.9	33.1
MD3J→8J	1.2E3	1.3	11.8	MD3J→P2	1.5E9	0.9	30.4
MD4J→8J	9.1E4	1.3	13.9	MD3J→P3	2.7E8	0.9	30.3
MD4J→9J	15.9	2.1	10.2	MD4J→P4	6.0E13	0.1	31.1
MD5J→9J	4.2E3	1.7	12.8	MD4J→P5	2.0E13	0.8	25.9
MD5J→10J	41.4	2.1	12.3	MD5J→P6	3.4E11	0.5	30.9
MD6J→9J	15.1	2.8	20.0	MD5J→P7	1.3E10	0.9	29.9
MD6J→10J	11.3	2.5	13.5	MD6J→P8	1.4E8	1.3	29.5
MD7J→2J	5.0E-2	2.7	9.2	MD6J→P9	8.3E9	0.9	30.3
MD7J→3J	6.6	2.2	12.8	MD7J→P10	2.4E9	0.9	29.4
MD8J→3J	59.4	1.8	12.3	MD7J→P11	2.4E8	1.3	29.4
MD8J→4J	1.2E3	1.7	13.9	MD8J→P12	5.7E9	1.0	32.2
MD9J→4J	0.5	2.5	9.7	MD8J→P13	2.7E10	0.5	30.7
MD9J→5J	1.6E2	2.0	12.0	MD9J→P14	1.1E8	1.3	28.3
MD10J→5J	1.4E2	2.1	10.7	MD10J→P15	8.4E10	1.0	30.2
MD10J→6J	4.1E4	1.7	12.4	MDMJ→P16	3.6E9	0.9	32.7

^a units of *A* and *E_a* are s⁻¹ and kcal/mol, respectively. $k(T) = AT^n \exp(-E_a/RT)$.

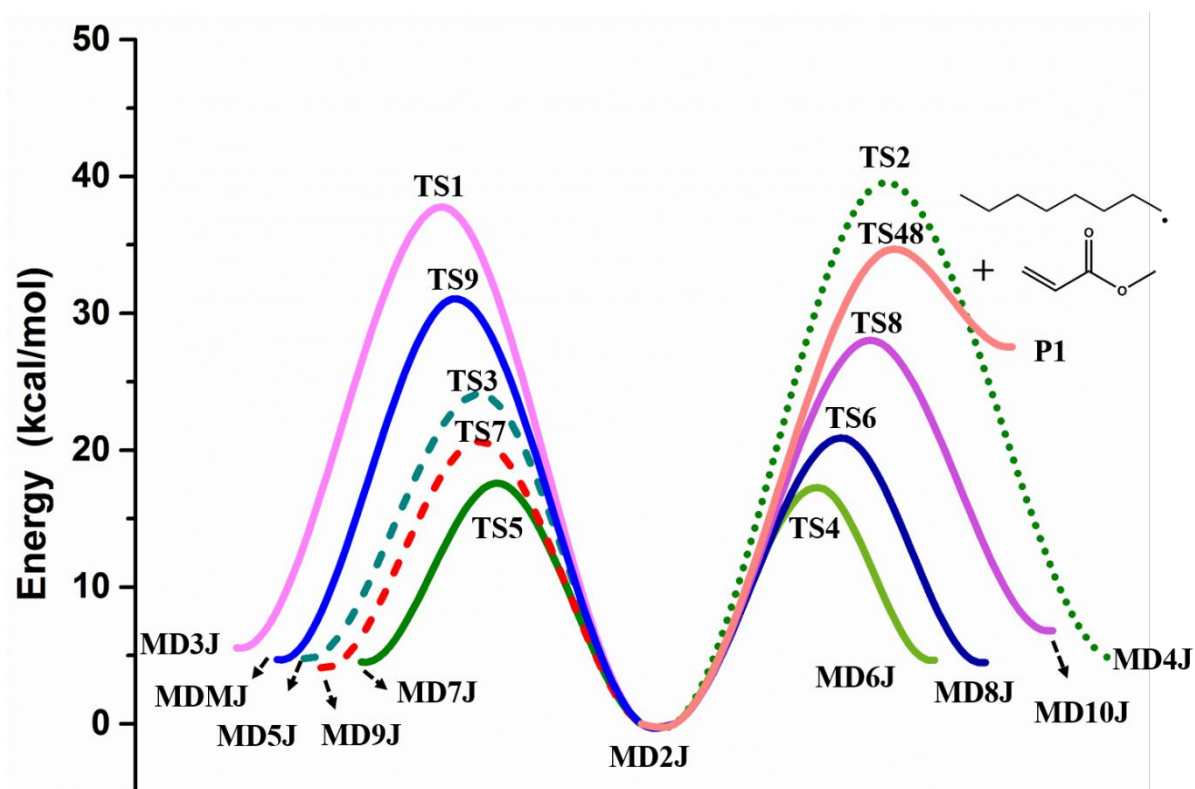


Fig. 1. Potential energy surface for the isomerization and β -scission reactions of MD2J at the ONIOM [QCISD(T)/CBS:DFT]/M06-2X/6-311++G(d,p) level.

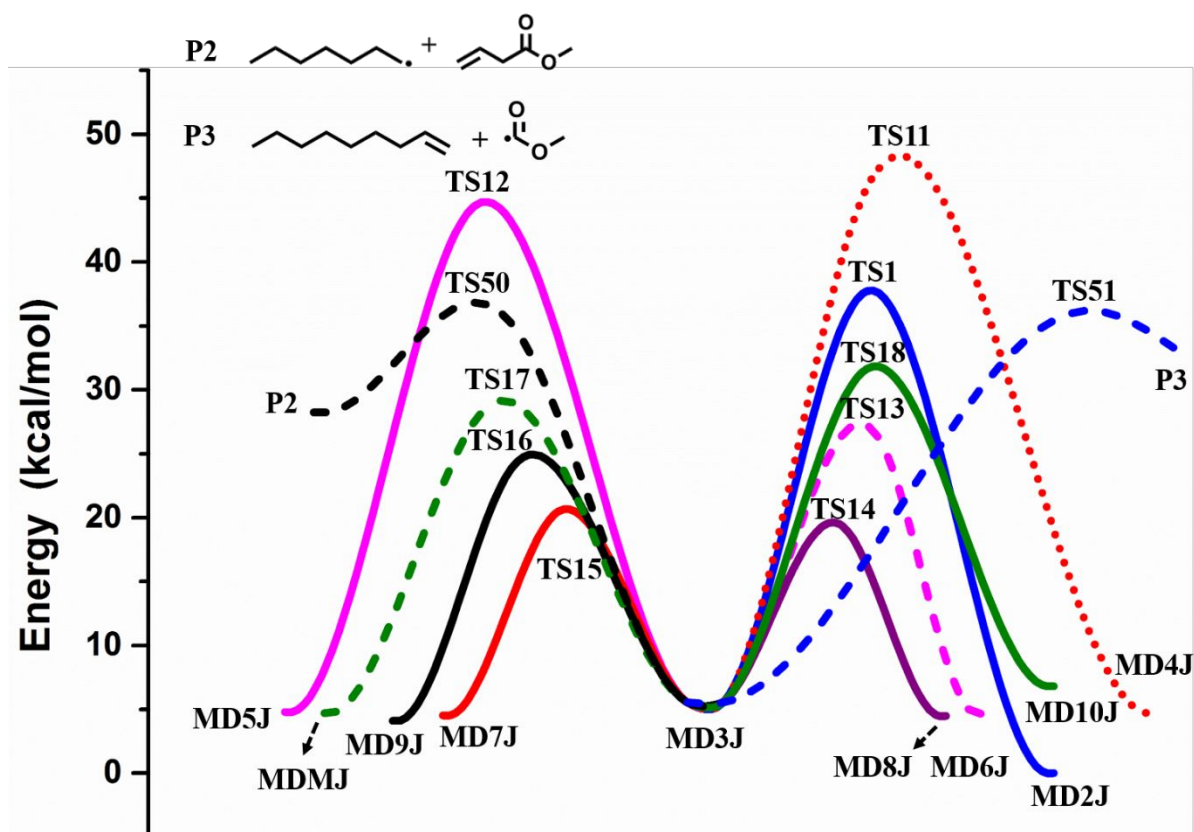


Fig. 2. Potential energy surface for the isomerization and β -scission reactions of MD3J at the ONIOM [QCISD(T)/CBS:DFT]/M06-2X/6-311++G(d,p) level.

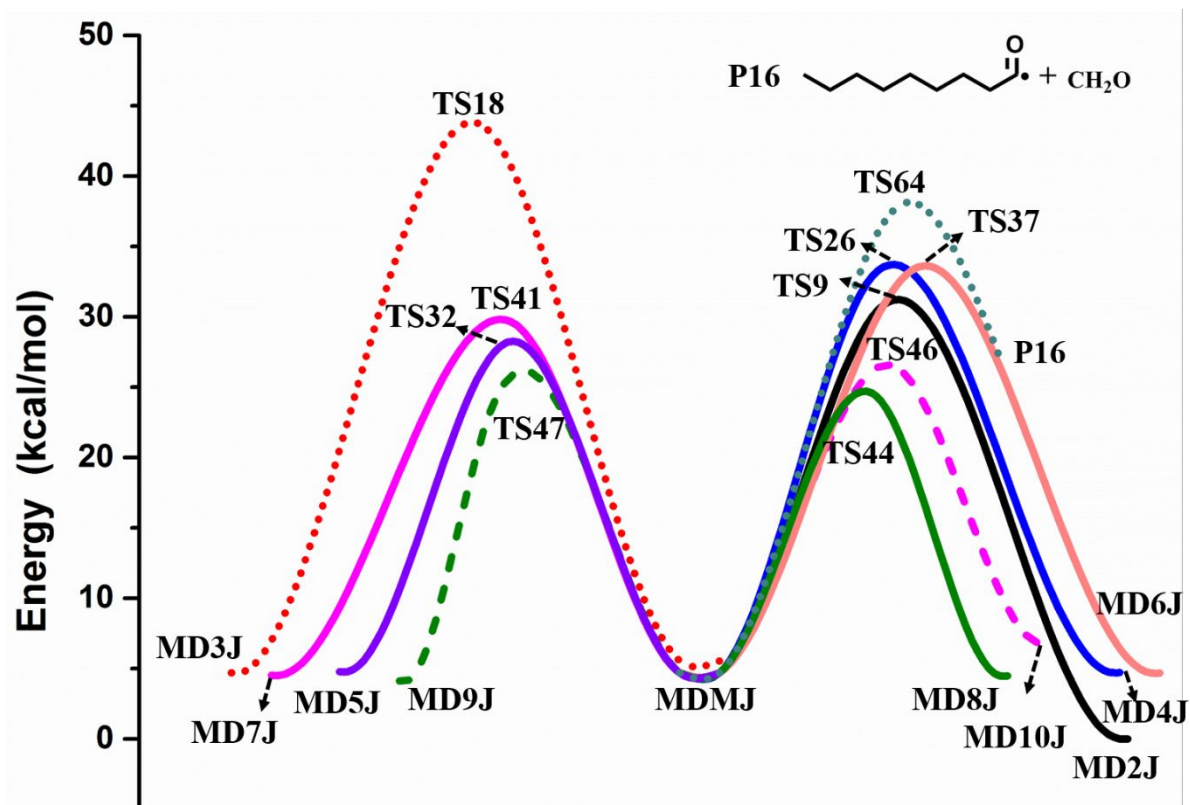


Fig. 3. Potential energy surface for the isomerization and β -scission reactions of MDMJ at the ONIOM [QCISD(T)/CBS:DFT]/M06-2X/6-311++G(d,p) level.

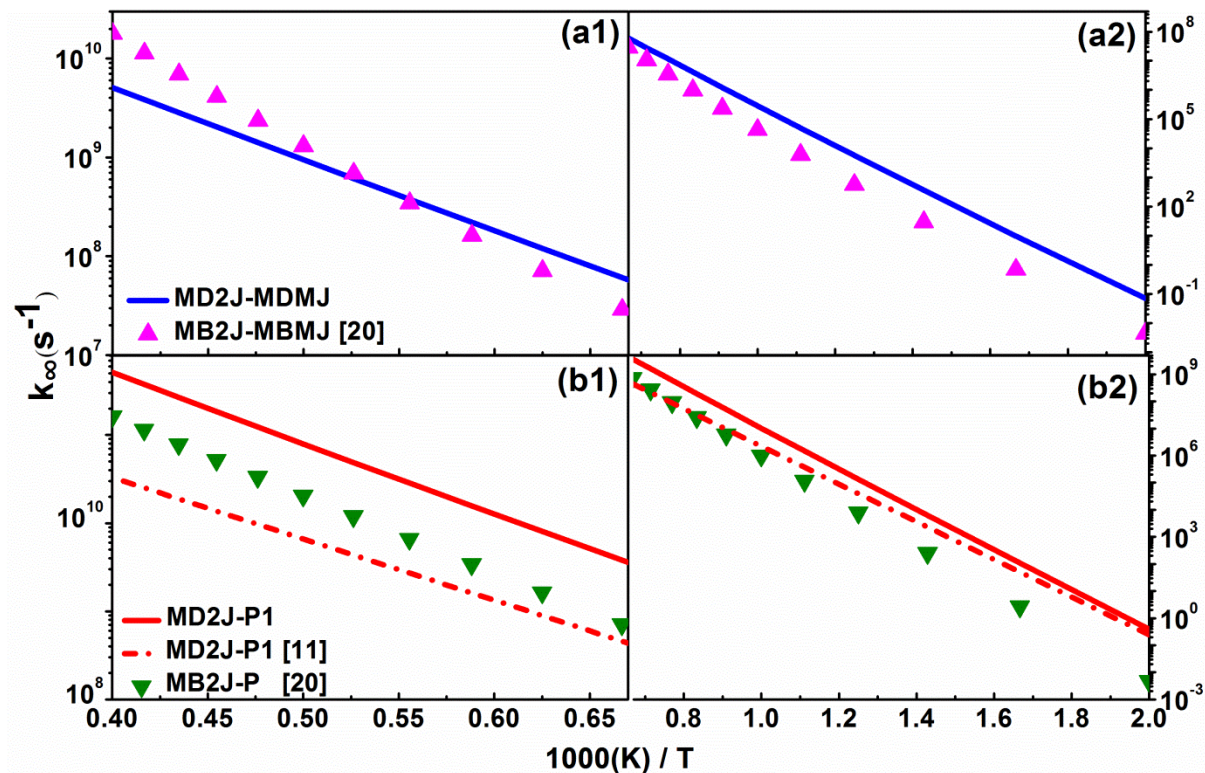


Fig. 4. High-pressure limit rate coefficients for the representative (a) isomerization and (b) dissociation reactions of MD2J. Rate coefficients of relevant reactions for MD¹¹ and MB²⁰, specific to methyl esters, are shown for comparison.

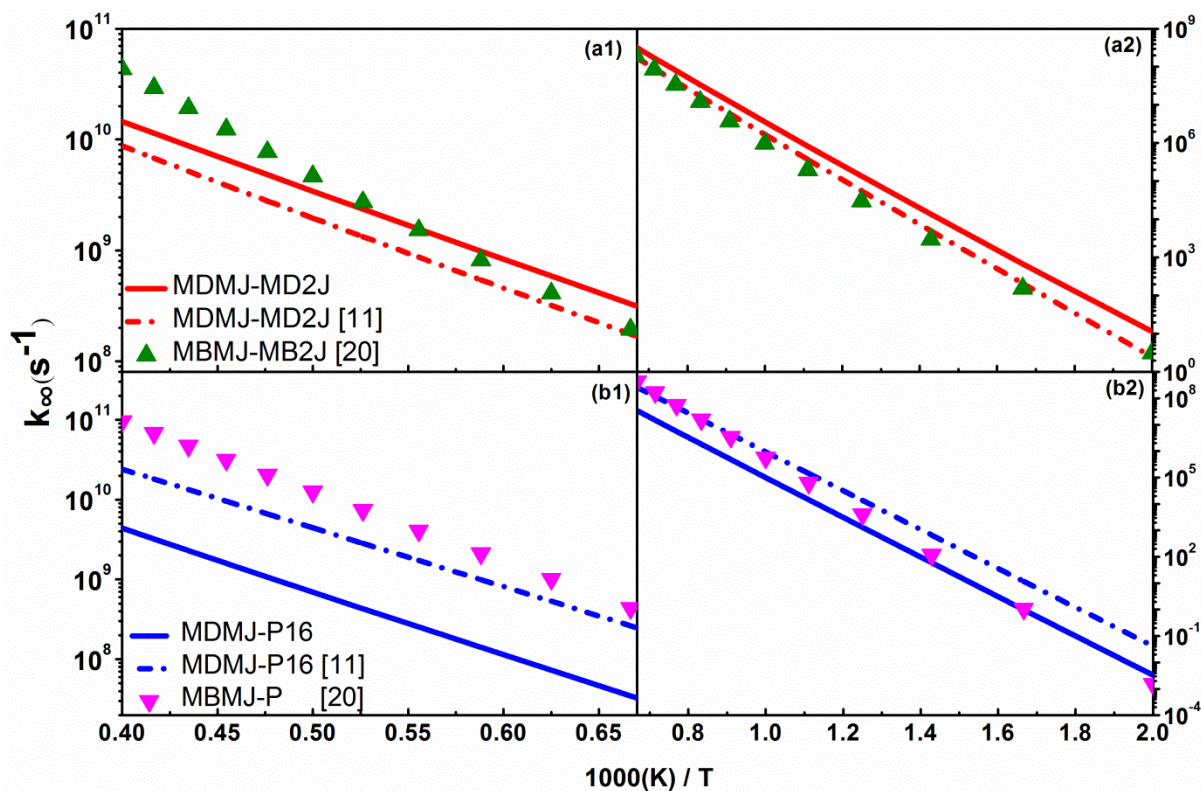


Fig. 5. High-pressure limit rate coefficients for the representative (a) isomerization and (b) dissociation reactions of MDMJ radical. Rate coefficients of relevant reactions for MD¹¹ and MB²⁰, specific to methyl esters, are shown for comparison.

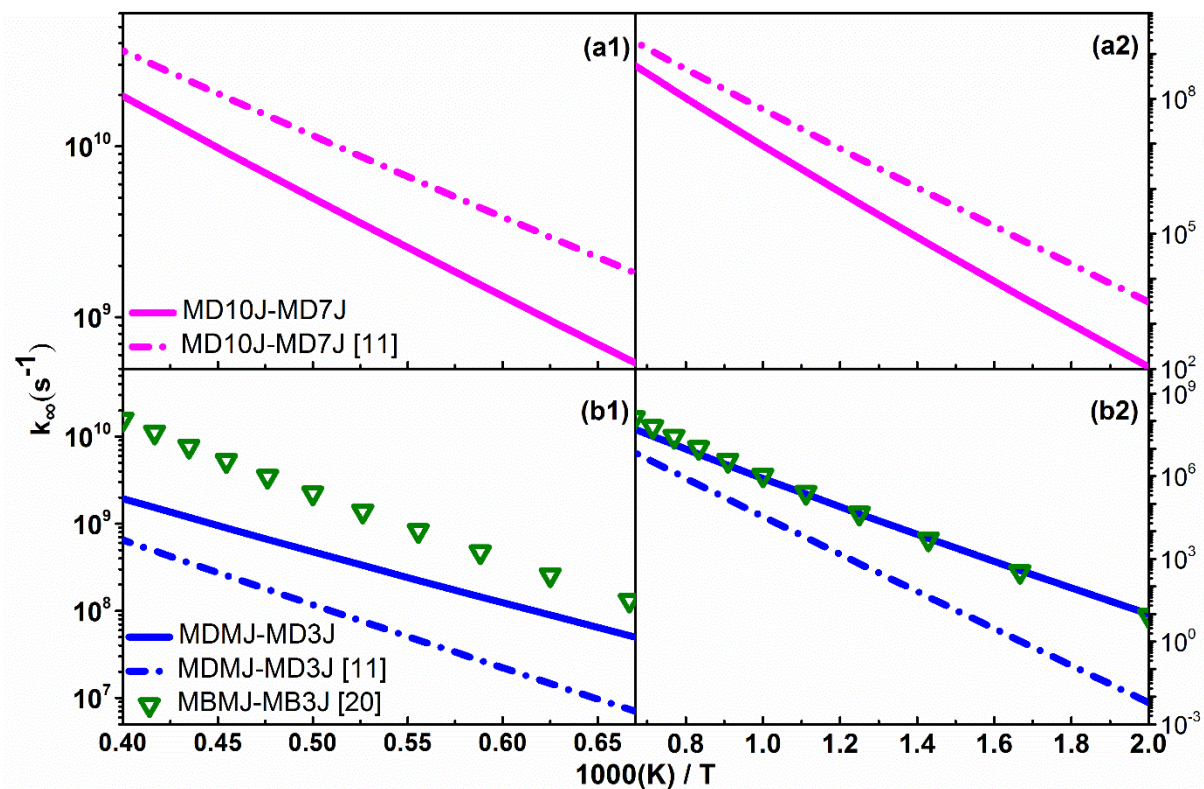


Fig. 6. Illustration of difference for the isomerization reactions of (a) MDMJ→MD3J and (b) MD10J→MD7J between the calculated and estimated rate coefficients at high pressure limit

11 20

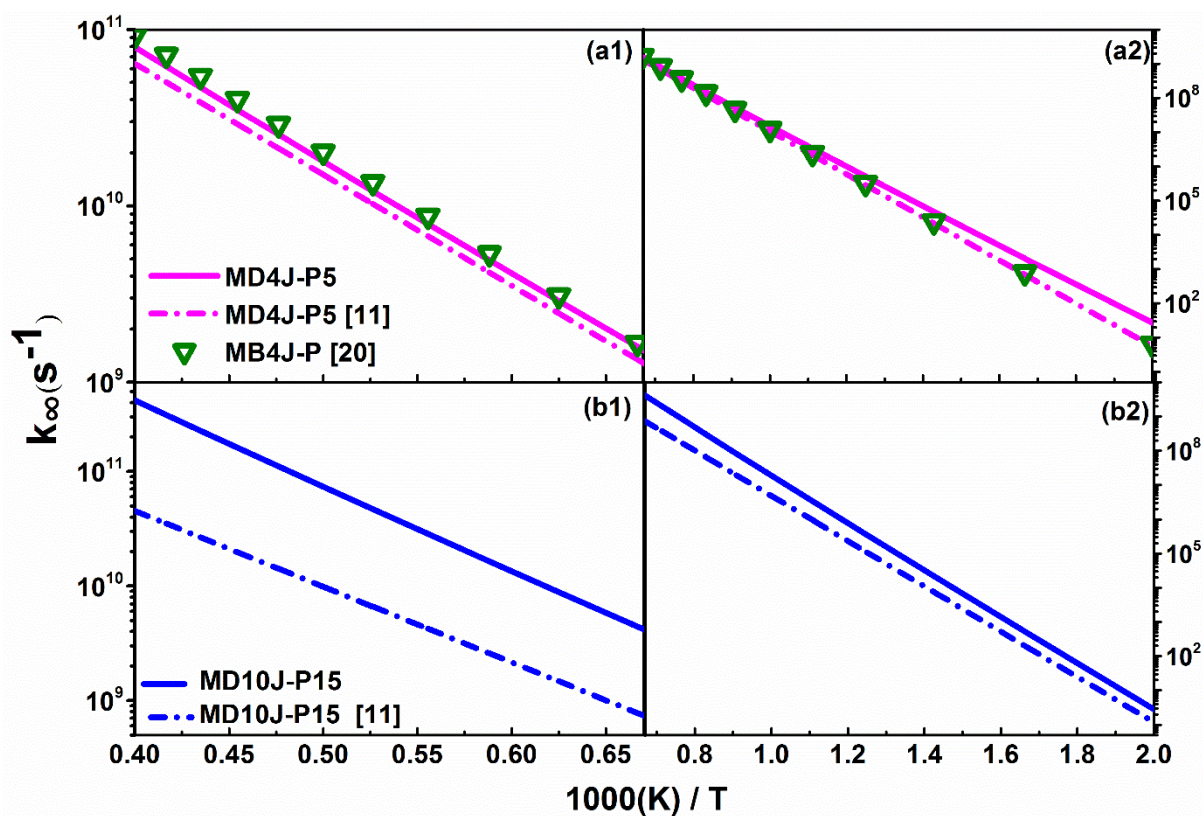


Fig. 7. Illustration of difference for the isomerization reactions of (a) MD4J \rightarrow P5, (b) MD10J \rightarrow P15 between the calculated and estimated rate coefficients at high pressure limit^{11 20}.

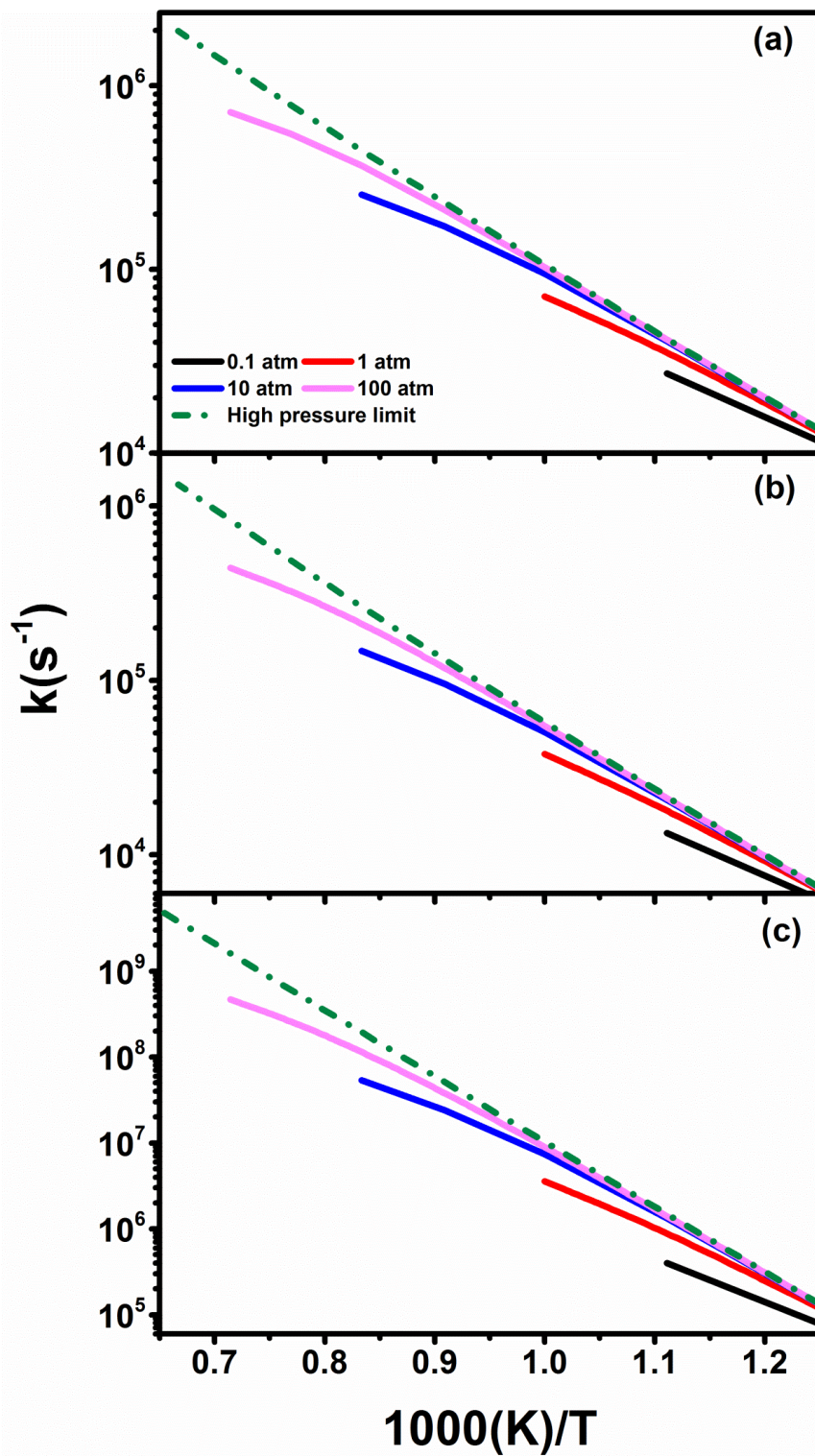


Fig. 8. The temperature and pressure-dependent rate coefficients for kinetically favorable reactions of MD2J. (a) MD2J-MD6J, (b) MD2J-MD7J, (c) MD2J-P1.

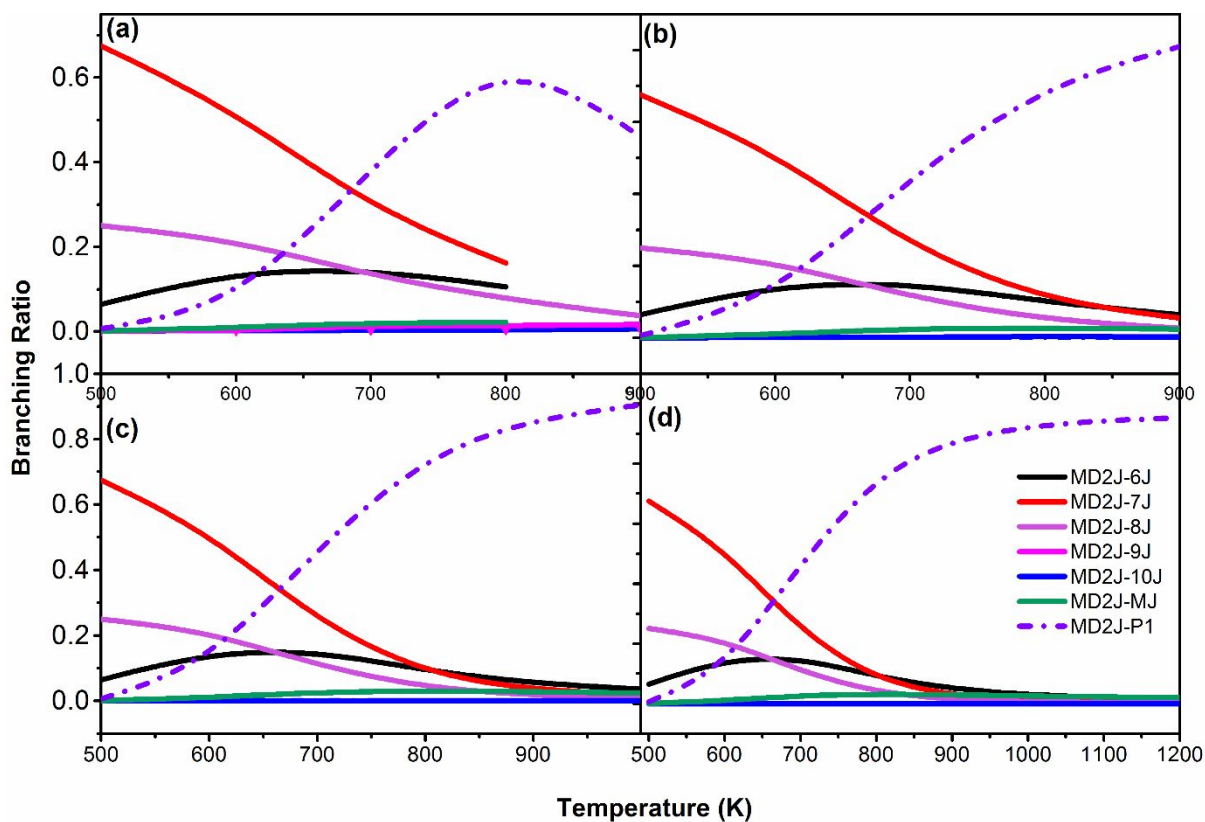


Fig. 9. Temperature-dependent branching ratios for main reactions of MD2J at 0.1atm, 1atm, 10atm and 100 atm, respectively.

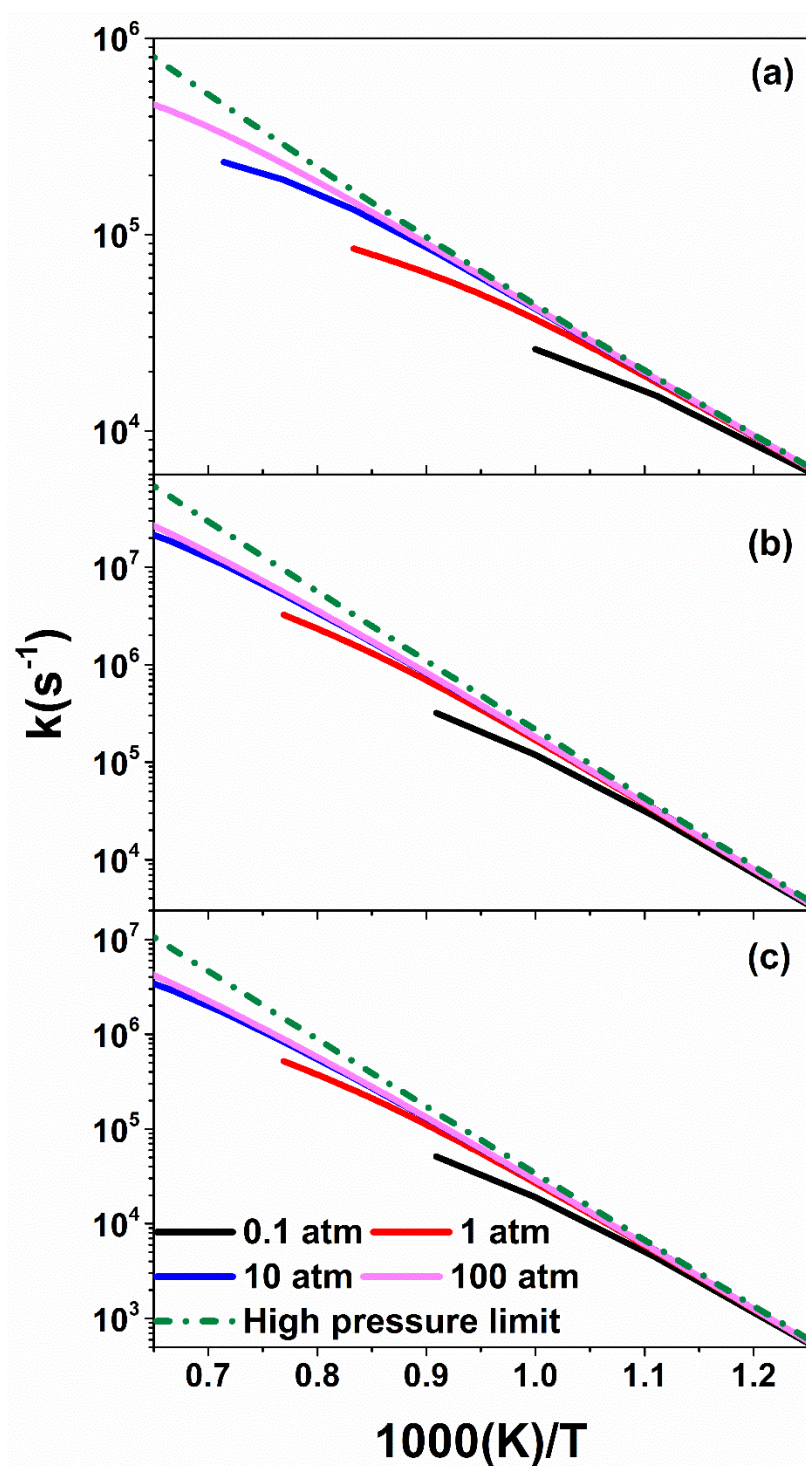


Fig. 10. The temperature and pressure-dependent rate coefficients for kinetically favorable reactions of MD3J. (a) MD3J-MD7J, (b) MD3J-P2, (c) MD3J-P3.

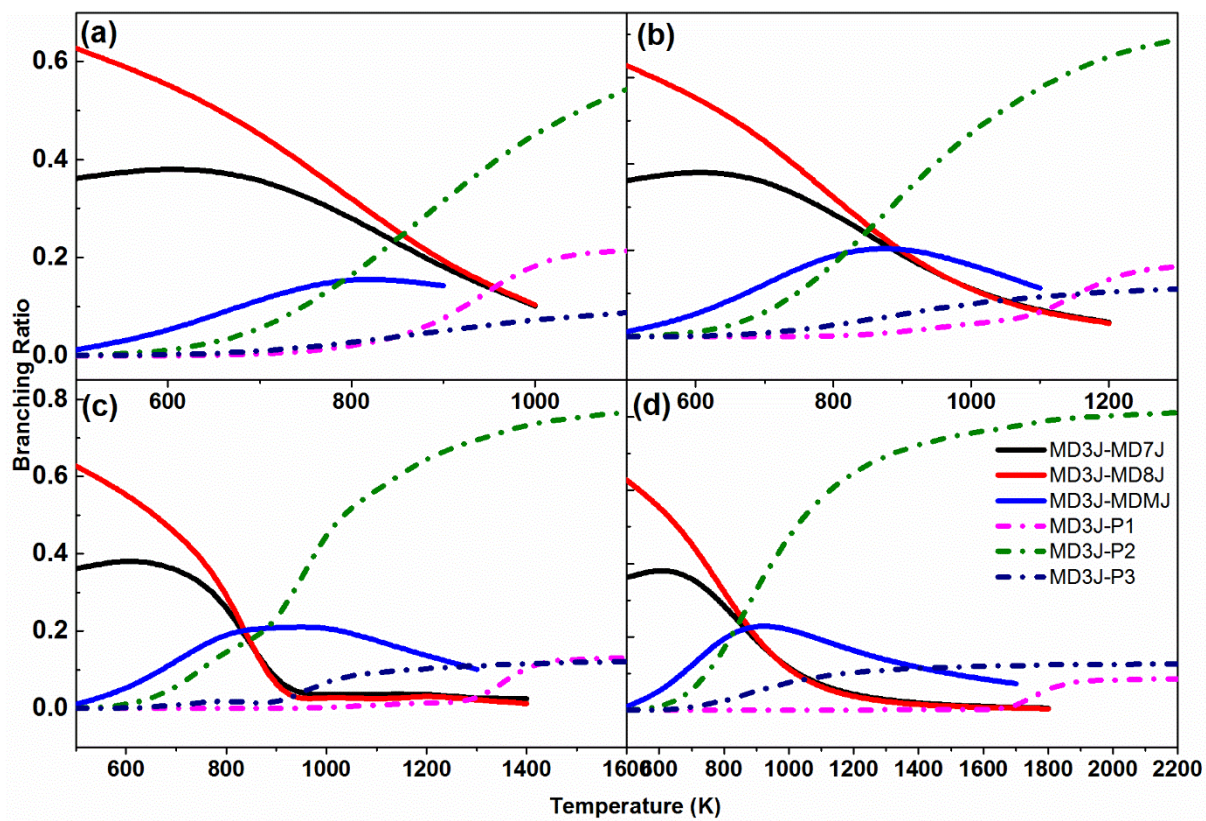


Fig. 11. Temperature-dependent branching ratios for main reactions of MD3J at 0.1 atm, 1 atm, 10 atm and 100 atm, respectively.

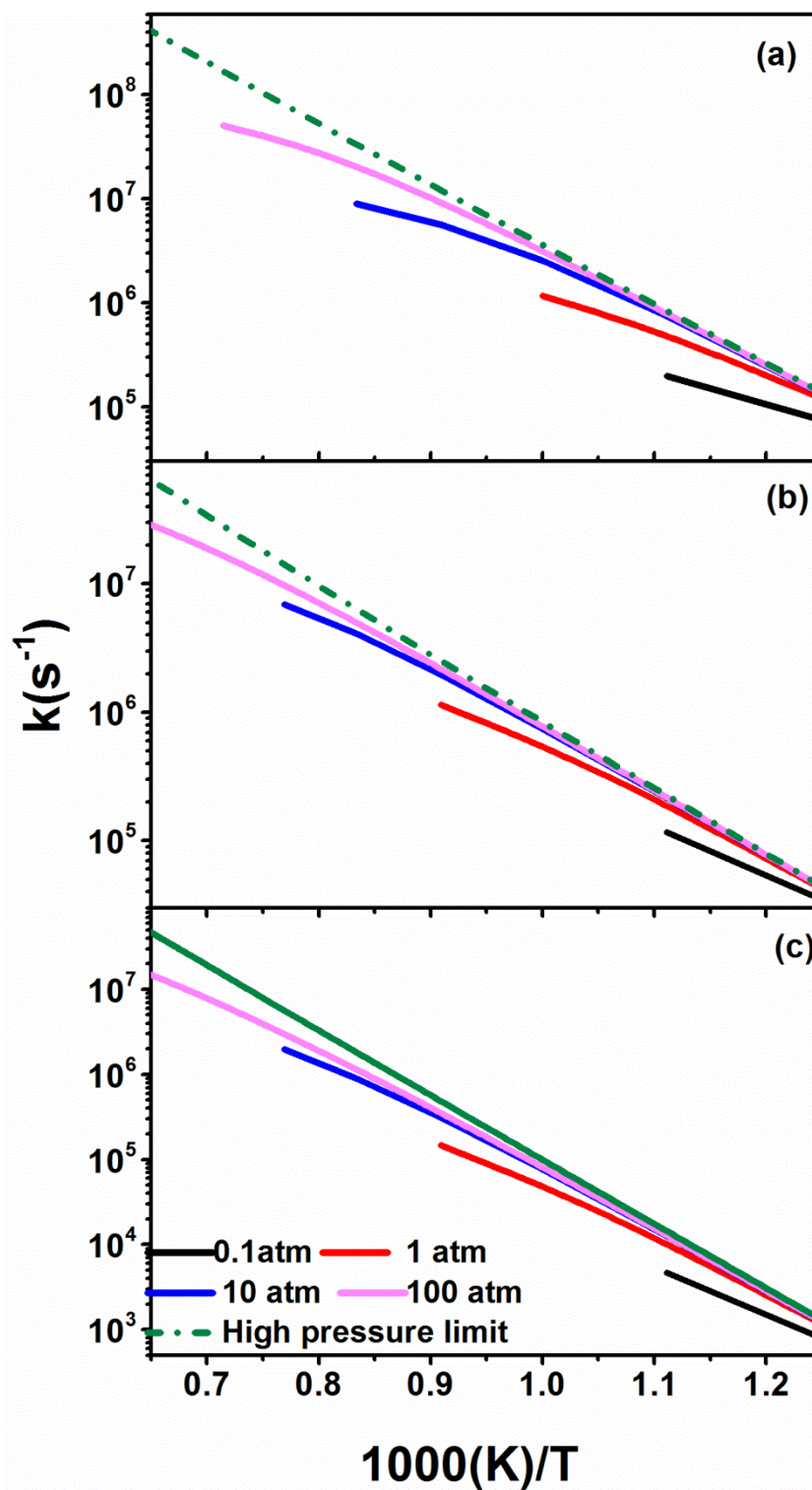


Fig. 12. The temperature and pressure-dependent rate coefficients for kinetically favorable reactions of MDMJ. (a) MDMJ-MD2J, (b) MDMJ-MD3J, (c) MDMJ-P16.

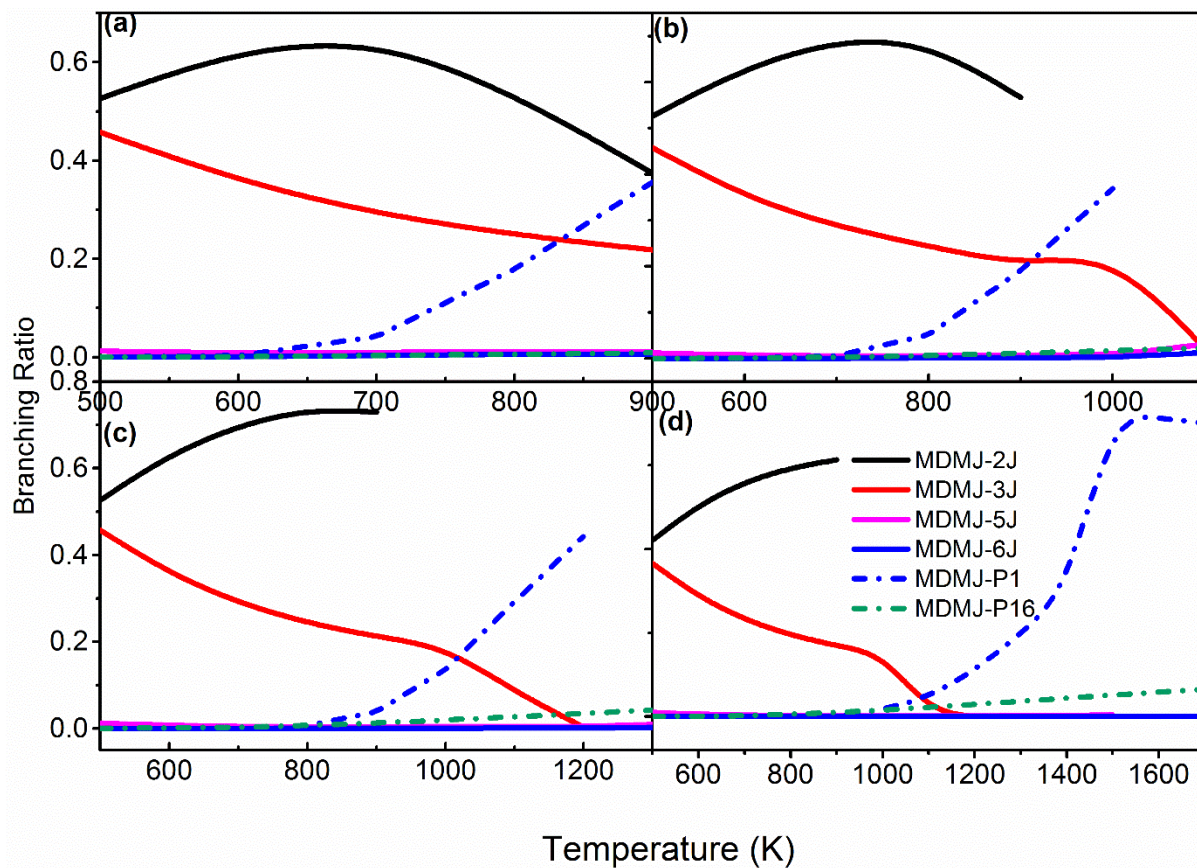


Fig. 13. Temperature-dependent branching ratios for main reactions of MDMJ at 0.1 atm, 1 atm, 10 atm and 100 atm, respectively.